Proc. of the 1995 Int. Conf. on Intelligent Robots and Systems, IROS'95, August 5-9, 1995, Pittsburgh, PA.

On the Interaction of Flexible Modes and On-off Thrusters in Space Robotic Systems

E. Martin E. Papadopoulos J. Angeles

Department of Mechanical Engineering and Centre for Intelligent Machines,
McGill University, Montreal, Quebec, Canada, H3A 2A7

Abstract

Space manipulators mounted on a on-off thruster-controlled base are envisioned to assist in the assembly and maintenance of space structures. When handling large payloads, manipulator joint and link flexibility become important, for it can result in payload-attitude controller fuel-replenishing dynamic interactions. In this paper, the dynamic behavior of a flexible-joint manipulator on a free-flying base is approximated by a single-mode mechanical system, while its parameters are matched with available space-manipulator data. Describing functions are used to predict the dynamic performance of three alternative controller/estimator schemes, and to conduct a parametric study on the influence of key system parameters. Design guidelines and a particular state-estimator are suggested that can minimize such undesirable dynamic interactions as well as thruster fuel consumption.

1 Introduction

Robotic devices in orbit will play an important role in space exploration and exploitation. The mobility of such devices can be enhanced by mounting them on free-flying bases, controlled by on-off thrusters. Such robots introduce a host of dynamic and control problems not found in terrestrial applications. When handling large payloads, manipulator joint or structural flexibility becomes important and can result in payload-attitude controller fuel-replenishing dynamic interactions. Such interactions may lead to control system instabilities, or manifest themselves as limit cycles [1].

A common approach to the design of thruster-based control systems is to consider single-axis, rigid-body motion, and to define a thruster switching logic using phase-plane techniques. As reported in [2], considerable research effort has been devoted on the attitude control problem of a *flexible spacecraft* using continuous control laws, and more recently, using on-off thrusters [3, 4, 5, 6]. All these methods assume knowledge of precomputed approximate or exact spacecraft flexible modes and frequencies. However, for a space robotic system, or for a multitask servicer such as the Space Shuttle, natural frequencies are continuously changing with manipulator configuration and payload. Therefore, these control methods cannot be directly implemented in space robotic systems.

The CANADARM-Space Shuttle system is the only operational space robotic system. Its flexible modes can have rather low frequencies that can be excited by Reaction Control System (RCS) activity. The performance degradation of the RCS due to the deployment of a *flexible payload*, with or without the CANADARM, was studied in [7]. After conducting extensive simulations, it was concluded that the judicious selection of control parameter values and careful operational procedures, based on a knowledge of payload structural characteristics, reduces dynamic interactions. The describing function method was used to analyze the problem of payload deployment by means of a tilt table [8]. Stability maps were obtained and compared to simulation results to validate the describing function analysis. A new design for the RCS was developed to reduce the impact of large measurement uncertainties in the rate signal during attitude control, as reported in [9]. The performance of the RCS is increased significantly for rigid-body motion. However, the flexibility problem was not addressed, and it is only mentioned that the likelihood of causing structural problems diminishes by reducing the number of required firing [9]. Currently, the method for resolving these problems consists of performing extensive simulations. If dynamic interactions occur, corrective actions are taken, which would include adjusting the RCS parameter values, or simply changing the operational procedures [7, 8]. The consequences of such interactions can be problematic, since fuel is an unavailable resource in space; hence, classical attitude controllers must be improved to reduce the possibility of such dynamic interactions.

In this work, these dynamic interactions were modeled using simple models, aiming at obtaining an understanding of the relative significance of system parameters. This understanding is of great importance to our main objective, which is to develop control methods that are intended to reduce the undesired effects of these dynamic interactions. In this paper, a single mode mechanical system is used to approximate the dynamic behavior of a two-flexible-joint manipulator mounted on a three-DOF base. Three alternative controller/estimator models are developed, and the describing function technique is used to conduct a parametric study on the influence of key system parameters. A particular state-estimator model and design guidelines are suggested that can minimize such undesirable dynamic interactions as well as thruster fuel consumption. An example and typical simulation results are also presented.

2 Modeling

The dynamics model of a two-flexible-joint planar manipulator mounted on a free-floating base was developed using a Lagrangian formulation under the assumption that all link and joint flexibilities are lumped at the joints [10]. This is reasonable, since joint flexibility is more significant than link flexibility in this kind of system. Each flexible joint is modeled as a torsional spring in parallel to a torsional dashpot. Using linearization techniques, the natural frequency expressions for this system were obtained as a function of the configuration of the manipulator, [10].

However, the dynamics of a simple two-flexible-joint planar manipulator is rather complicated; it is preferable to employ a simplified model to analyze the problem stated in Section 1. We can replace the manipulator of Fig. 2(a) with an equivalent two-mass-spring-dashpot system, as shown in Fig. 2(b). By a proper selection of the spring stiffness k and the damping coefficient c, the resonant frequency of the simplified system can be matched to the first one of the original system. Therefore, a similar relative motion of the payload with respect to the base can be obtained.

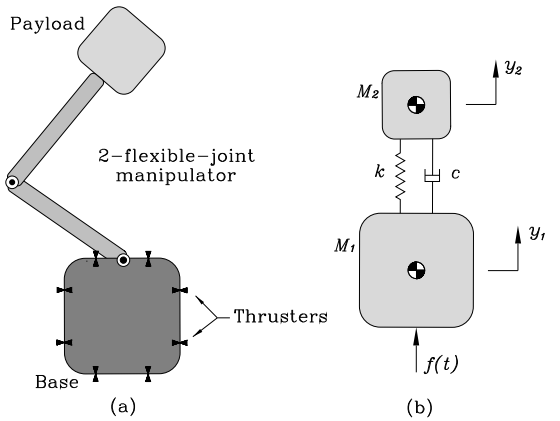

Fig. 1. Flexible manipulator replaced by a spring and a dashpot: (a) Two-link manipulator on a floating base; (b) Simplified two-mass system.

The equations of motion for the system shown in Fig. 2(b) can be readily derived as

$$M_1\ddot{y}_1 + c(\dot{y}_1 - \dot{y}_2) + k(y_1 - y_2) = f(t) \qquad (1a)$$
$$M_2\ddot{y}_2 - c(\dot{y}_1 - \dot{y}_2) - k(y_1 - y_2) = 0\ , \qquad (1b)$$

where M_1 is the mass of the base, M_2 the mass of the payload, y_1 the position of the base, y_2 the position of the payload, k the spring stiffness, c the damping coefficient, $f(t) = Bu$, with B the magnitude of the force developed by the thrusters, and u is the command of the thrusters, either $+1$, 0 or -1.

The overall motion of the system can be decomposed into a rigid-body motion of the system CM, and a flexible-body motion around the center of mass, defining the resonant frequency ω_n, the damping ratio ζ, and the reduced mass μ as

$$\omega_n = \sqrt{\frac{k}{\mu}}\ , \qquad \zeta = \frac{c}{2\sqrt{\mu k}}\ , \qquad \mu = \frac{M_1 M_2}{M_1 + M_2}\ . \quad (2)$$

From Eq.(2), we obtain the system stiffness k and damping coefficient c, as

$$k = \mu\omega_n^2, \qquad c = 2\mu\zeta\omega_n\ . \qquad (3)$$

Therefore, using Eq.(3), k and c can be chosen to match a specific resonant frequency ω_n and a damping ratio ζ for given masses M_1 and M_2.

In order to write the system equations (1) in state-space form, we define: $x_1 = y_1$, $x_2 = \dot{y}_1$, $x_3 = y_2$ and $x_4 = \dot{y}_2$. Making use of Eqs.(2) and (3), and defining the state vector as $\mathbf{x} = [x_1, x_2, x_3, x_4]^T$, Eqs.(1) are written as

$$\dot{\mathbf{x}} = \mathbf{A}\mathbf{x} + \mathbf{b}u \qquad (4a)$$

where

$$\mathbf{A} = \begin{bmatrix} 0 & 1 & 0 & 0 \\ -\frac{\beta}{1+\beta}\omega_n^2 & -\frac{\beta}{1+\beta}2\zeta\omega_n & \frac{\beta}{1+\beta}\omega_n^2 & \frac{\beta}{1+\beta}2\zeta\omega_n \\ 0 & 0 & 0 & 1 \\ \frac{1}{1+\beta}\omega_n^2 & \frac{1}{1+\beta}2\zeta\omega_n & -\frac{1}{1+\beta}\omega_n^2 & -\frac{1}{1+\beta}2\zeta\omega_n \end{bmatrix} \qquad (4b)$$

and

$$\mathbf{b} = [\ 0 \quad a_0 \quad 0 \quad 0\ ]^T\ . \qquad (4c)$$

The available acceleration of the base a_0 and the mass ratio β are given by

$$a_0 = B/M_1, \qquad \beta = M_2/M_1\ . \qquad (5)$$

The required outputs are either y_1, or y_1 and $\dot{y}_1$, and are obtained using

$$y = y_1 = \mathbf{c}^T\mathbf{x} = [\ 1 \quad 0 \quad 0 \quad 0\ ]^T\,\mathbf{x} \qquad (6a)$$

$$\mathbf{y} = [\ y_1 \quad \dot{y}_1\ ]^T = \mathbf{C}\mathbf{x} = \begin{bmatrix} 1 & 0 & 0 & 0 \\ 0 & 1 & 0 & 0 \end{bmatrix}\mathbf{x}. \qquad (6b)$$

3 Control

The technology currently available does not allow the use of proportional thruster valves in space, and thus, the classical PD and PID control laws cannot be used. Therefore, spacecraft attitude and position are controlled by the use of on-off thruster valves, that introduce nonlinearities.

The usual scheme to control a spacecraft with on-off thrusters is by the use of the error phase plane, defined as having the spacecraft attitude error e and error rate $\dot{e}$ as coordinates. The on-and-off switching is determined by switching lines in the phase plane and can become complex, as for example the phase plane controller of the Space Shuttle [7]. To simplify the switching logic, two switching lines with equations $e + \lambda\dot{e} = \pm\delta$ have been used, see Fig. 3. The deadband limits $[-\delta,\ \delta]$ are determined by attitude limit requirements, while the slope of the switching lines, by the desired rate of convergence towards the equilibrium and by the rate limits. This switching logic can be represented as a relay with a deadband, where the input is $e + \lambda\dot{e}$, the left-hand side of the switching-line equations, see Fig. 3.

To compute the input to the controller, the position and the velocity of the system base are required. Using current space technology, both states can be obtained

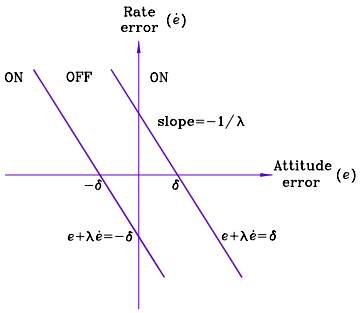

Fig. 2. Switching logic in the error phase plane.

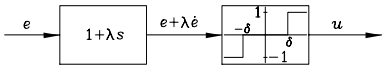

Fig. 3. Controller block.

by sensor readings. However, it can happen that only the attitude is available and then, the velocity must be estimated. In this paper, three cases are considered. For Case 1, we assume that both signals are available and are simply filtered to eliminate high frequency noise. To this end, second-order filters are used, represented by the transfer function $G_f(s)$, namely,

$$G_f(s) = \frac{\omega_f^2}{s^2 + 2\zeta_f\omega_f s + \omega_f^2} \tag{7}$$

The cutoff frequency ω_f must be chosen to filter high frequencies such that it does not slow down the response of the system by reducing its bandwidth. Since the exact frequency content of noise is not known, we use ω_f as a parameter in our study to examine its influence on system performance. The damping term ζ_f in Eq.(7) is chosen to be 0.707, which gives good performance, since it is relatively fast, with zero resonant peak. The complete model required for analysis is obtained by grouping the blocks for the controller, the plant and the state estimator, as displayed in Fig. 3. For cases 2 and 3, we assume that only the position is available from sensors, and, to obtain the velocity, we use two different state estimators.

In Case 2, a controller-plant-estimator configuration similar to the one used on the Space Shuttle is employed, see also [7, 8]. A differentiator combined with a second-order filter is used to obtain a velocity estimate, see Fig. 3. The differentiation of a noisy signal is usually not recommended because it amplifies noise. However, in this case, it is possible to use a scheme where only the flexible part of the motion needs to be differentiated. This means that, at the limit, for a rigid system, no differentiation is necessary. This state estimator can give very good results when flexibility is low. The differentiator-filter is given by $sG_{se}(s)$ where

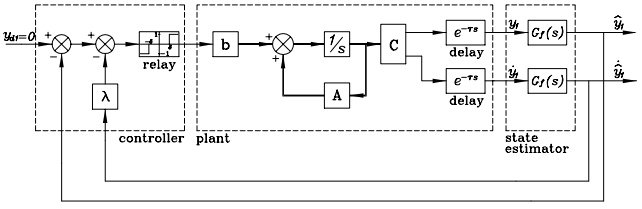

Fig. 4. Case 1: model with position and velocity filters.

$$G_{se}(s) = \frac{\omega_{se}^2}{s^2 + 2\zeta_{se}\omega_{se}s + \omega_{se}^2} \tag{8}$$

The position feedback is also low-pass-filtered according to Eq.(7), with $\zeta_f = 0.707$ and ω_f free to vary. The cutoff frequency for the differentiator-filter is chosen as $\omega_{se} = 0.2513$ rad/s and the damping ratio as $\zeta_{se} = 0.707$. These values correspond to the ones used on the Space Shuttle, see [7, 8].

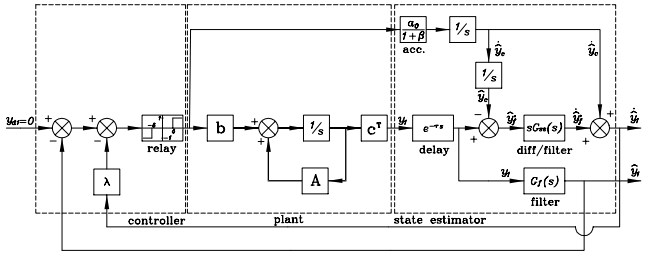

Fig. 5. Case 2: model with a velocity estimator and a position filter.

For Case 3, an asymptotic state observer is used to obtain an estimate for the position and the velocity from a position measurement [11]. The configuration corresponding to this case is depicted in Fig. 3. The observer gain $\mathbf{k}$ is computed such that two poles of the error state equations are placed on the negative real axis of the real-imaginary plane, at the chosen frequency ω_f, while the other two are placed symmetrically about the negative real axis at the same frequency, but with $\zeta_f = 0.707$.

In all three cases, a time delay τ has been included to account for the delay between the time a sensor reads a measurement, and the time this measurement is used. Since this delay is more significant than the delay of turning on or off the thrusters, only a sensor time delay is included.

4 Frequency Domain Analysis

Since the attitude controller assumes use of on-off thrusters, which are nonlinear devices, the system cannot be adequately analyzed through the application of linear analysis methods. This problem is tackled using the describing function method which can predict the existence of limit cycles in nonlinear systems [12, 13].

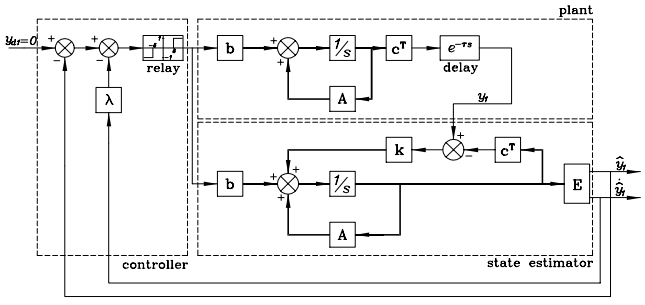

Fig. 6. Case 3: model with an asymptotic state estimator.

In order to use this method, a system must be partitioned in a linear and a nonlinear part. Then, it is transformed into the configuration in Fig. 4. $G(j\omega)$ is the frequency response of all the linear elements in the system and $N(A,\omega)$ is the describing function of the nonlinearity which is tabulated in many books, see for example [13]. For the three cases described in the previous section, it is always possible to reduce the block diagrams in the configuration of Fig. 4.

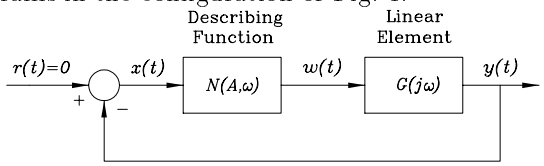

Fig. 7. A feedback system with its nonlinear part replaced by a corresponding describing function.

The characteristic equation of the system depicted in Fig. 4 can be written as

$$G(j\omega) = -\frac{1}{N(A,\omega)} \ . \qquad (9)$$

The reader is refered to [12] and [13] for a detailed description of the method. In summary, if a given set of A and ω is a solution of Eq.(9), then the system exhibits a limit cycle of amplitude A and frequency ω. If the above equation has no solution, then the nonlinear system has no limit cycle. A convenient way to solve Eq.(9) consists of plotting both sides of the equation in the complex plane by varying A and ω, and observing whether the two curves intersect or not. An intersection point will provide the corresponding values of A and ω. Furthermore, one has to investigate the stability properties of the limit cycle and the general behavior of the system [13]. For example, Fig. 4 depicts three typical describing function plots encountered in this work, where the describing function N of the relay is a function of the gain A only. Figure 4(a) is typical of an unstable system where the motion diverges, none of the intersection points representing a stable limit cycle. Figure 4(b) depicts a system that sustains a limit cycle of amplitude A and frequency ω due to the dynamic interactions. Finally, Fig.4(c) shows a stable case where the motion reaches a small unavoidable limit cycle.

Figures 4(a) and (b) both correspond in high thruster activity. This behavior is not desirable in space missions, and should therefore be classified as unstable. In this paper, to draw stability conclusions, the following definition based on the rate of fuel consumption of the system is used.

Stability Definition

1. **Unstable system.** Describes either a system where the motion diverges, or a system where the motion reaches a limit cycle that is not contained inside the switching lines as for a rigid body limit cycle, resulting in a large rate of fuel consumption;

2. **Stable system.** Describes a system where the motion reaches an unavoidable limit cycle similar to a rigid body limit cycle, thus being contained between the switching lines, and resulting in a near-zero rate of fuel consumption as for a rigid system.

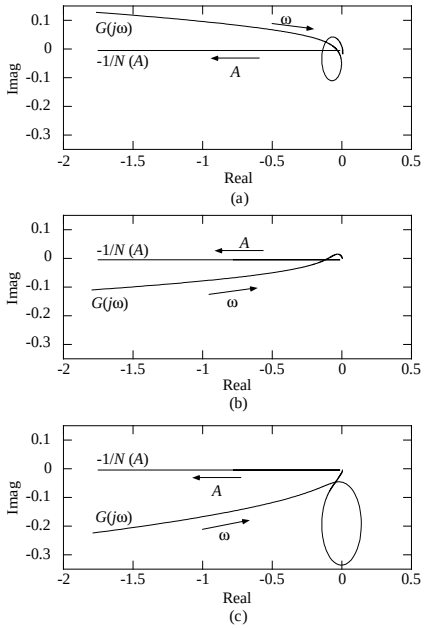

Fig. 8. Typical describing function plots: (a) Unstable system; (b) Limit cycling system; and (c) Stable system.

5 Parametric Studies and Results

Using the describing function method, a parametric study was undertaken to investigate the significance of key system parameters. The three cases presented in Section 3 are analyzed using the fixed parameter values of Table 5, and the range of parameter values of Table 5, both being based on available space manipulator data [10].

The frequency expressions for a planar two-flexible-joint manipulator derived in [10] where used to obtain the natural frequencies of the system in any configuration. The approximate system natural frequency ω_n is set equal to the first natural frequency of the two-flexible-joint manipulator system. Then, the range of ω_n, for the range of β and the specific configurations q_1 and q_3 used in the parametric study, are given in Table 5, where the ratio of the highest frequency to the lowest one is 5 to 1.

The results of the parametric study for Case 2 are illustrated with the use of stability maps, as those depicted in Fig. 5. Figure 5(a) shows the stability boundary for different cutoff frequencies ω_f of the second-

Table 1. Fixed-parameter values.

q_1	ζ	τ (s)	ω_{se} (rad/s)	ζ_f	ζ_{se}
135°	0.05	0.1	0.2513	0.707	0.707

Table 2. Free-parameter values.

β	$0.01 \leq \beta \leq 0.3$
λ (s)	$0.1 \leq \lambda \leq 10$
a_0 (m/s^2)	$0.0002 \leq a_0 \leq 0.02$
δ (m)	$0.001 \leq \delta \leq 0.1$
q_3	$-135°,\ -90°,\ -45°,\ 0°$
ω_f (rad/s)	$0.2513 \leq \omega_f \leq 4$

Table 3. Evaluation of the natural frequency ω_n (Hz) for $q_1 = 135°$.

β \ q_3	$-135°$	$-90°$	$-45°$	$0°$
0.01	0.255	0.170	0.136	0.127
0.05	0.128	0.090	0.075	0.071
0.1	0.097	0.072	0.062	0.059
0.15	0.083	0.065	0.057	0.054
0.2	0.076	0.061	0.054	0.052
0.25	0.071	0.058	0.052	0.050
0.3	0.067	0.056	0.051	0.049

order filter $G_f(s)$ given by Eq.(7). The region below such boundary represents a zone where the system is stable, while the region above corresponds to a zone of instability. As shown in the same figure, the stability zone can be increased by increasing the cutoff frequency ω_f. Analyzing the graphs in Fig. 5 in a similar way, guidelines for the design of attitude control systems when flexibility is a major concern, are obtained as follows

1. The cutoff frequency ω_f for the filters should be chosen as large as possible to avoid instability;

2. The velocity gain λ should be chosen as large as possible to avoid instability;

3. The acceleration of the base a_0 should be kept small for stability. Unstable types of behavior are more likely to occur for large a_0. However, one must be careful because the system can be unstable for a very low acceleration level, i.e., $a_0 = 0.0002$ m/s^2;

4. Deadband limits δ should be chosen as large as possible to avoid instability.

The upper limits of these parameters are set by design requirements or available hardware.

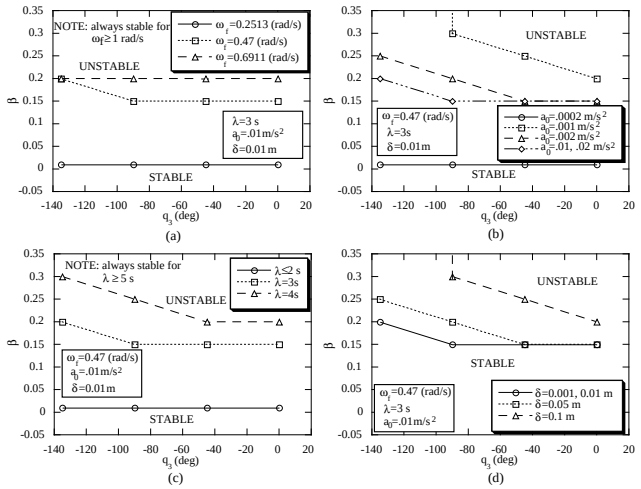

Fig. 9. Describing function stability maps for Case 2 showing: (a) the effect of the cutoff frequency ω_f; (b) the effect of the base acceleration a_0; (c) the effect of the velocity gain λ; and (d) the effect of the deadband limit δ.

The same conclusions are drawn when Case 1 is analyzed. However, in general, the performance of that case is worse than that for Case 2. To demonstrate this, the system configuration for Case 1 (Fig. 3) with parameters given in Tables 5 and 5, was used. Simulation results for an initial error of 0.05 m are shown in Fig. 5. Figures 5(b) and (c) show that thrusters are firing continuously, resulting in a high total fuel consumption of 486.7 fuel units, and a large rate of fuel consumption. Therefore, the system is classified as unstable. Moreover, the phase-plane trajectories in Fig. 5(a), show that a large limit cycle is reached due to the dynamic interactions.

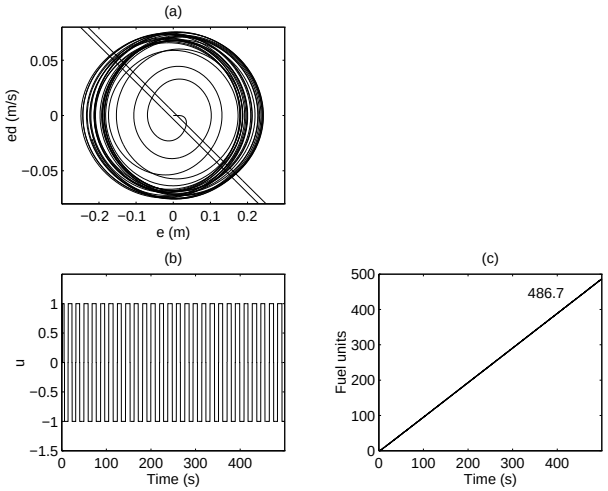

Fig. 10. Simulation results using the Case 1 model: (a) Spacecraft error phase plane; (b) Thruster command history; and (c) Fuel consumption.

If the model of Case 2 is simulated with the same parameter values, the results of Fig. 5 are obtained. Examining Figs. 5(b) and (c), we observe that thrusters are firing continuously, and that the total fuel consumption is quite high, namely, 155.2 fuel units. According to our stability definition, we can also conclude that the system is unstable. The same conclusion is reached with the describing function method, see Fig. 5(c) for $\lambda = 3$ s. Thus, the results corresponding to Cases 1 and 2 are both unstable, but the performance of Case 1 is worse than that for Case 2, since the fuel consumption is higher.

On the other hand, using the system configuration of Case 3, see Fig. 3, with the same parameters, provides very interesting results, as shown in Fig. 5. From Figs. 5(a) and (b), it can be seen that a limit cycle contained between the switching lines is reached, resulting in a stable system. One can note that the motion appears to be concentrated at the right side of Fig. 5(b) in a spiral motion due to the relative motion between the two masses, that damps out. Figs. 5(c) and (d) are

Table 4. Free-parameter values used for simulations.

β	λ (s)	a_0 (m/s^2)	δ (m)	ω_n (rad/s)	ω_f (rad/s)
.3	3	0.01	0.01	$2\pi(0.049)$	0.47

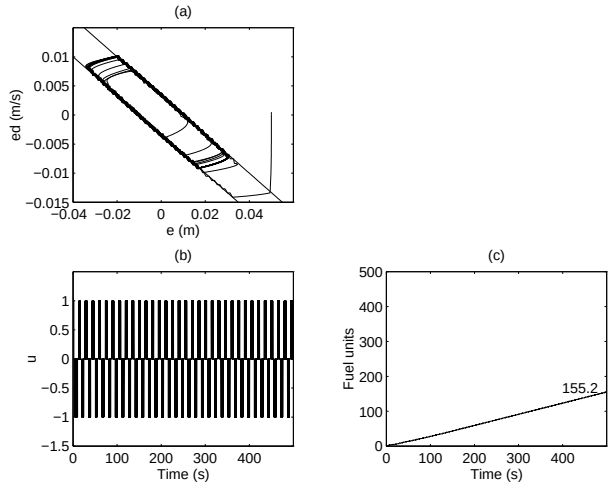

Fig. 11. Simulation results using the Case 2 model: (a) Spacecraft error phase plane; (b) Thruster command history; and (c) Fuel consumption.

also typical of a stable system, since the thrusters are not firing continuously and the fuel-consumption curve is flat, thereby resulting in a near-zero rate of fuel consumption, similar to that for a rigid body system. In this case, the total fuel consumption is very small; 6.6 fuel units only. Therefore, it is observed that the use of the proposed state estimator increases the performance of the control system significantly, and extends the system's operational life. In addition, using the describing function method, it can be shown that this estimator results in a system that is almost always stable for the whole range of parameters, resulting in significantly increased stability margins in comparison to Cases 1 and 2. Using simulation, it was shown that the performance of this estimator remains very good in the presence of noise and model uncertainties [10].

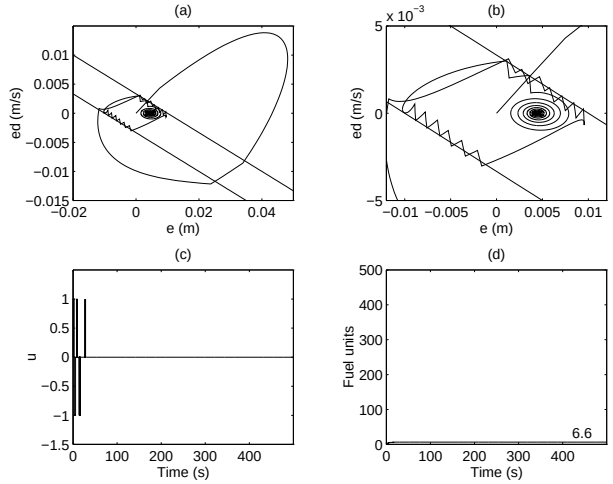

Fig. 12. Simulation results using the Case 3 model: (a) Spacecraft error phase plane; (b) Spacecraft error phase plane (zoom); (c) Thruster command history; and (d) Fuel consumption.

6 Conclusion

This work examined possible dynamic interactions between the attitude controller of a spacecraft and the flexible modes of a space manipulator mounted on it. A simplified model for the plant was used to analyze three different control/estimation schemes using the describing function method. The resonant frequency of this system is obtained by analyzing a planar two-flexible-joint manipulator mounted on a three-DOF spacecraft. Guidelines in the design of such systems resulted. This study also showed that the use of an asymptotic state estimator improves significantly the stability and the performance of the system.

Acknowledgements

The support of this work by the Fonds pour la Formation de Chercheurs et l'Aide à la Recherche (FCAR), and by the Natural Sciences and Engineering Council of Canada (NSERC) is gratefully acknowledged.

References

[1] Millar, R. A., and Vigneron, F. R., "Attitude Stability of a Pseudorate Jet-Controlled Flexible Spacecraft," *J. of Guid., Cont., and Dyn.*, Vol. 2, No. 2, 1979, pp. 111–118.

[2] Singh, G., Kabamba, P. T., and McClamroch, N. H., "Planar, Time-Optimal, Rest-to-Rest Slewing Maneuvers of Flexible Spacecraft," *J. of Guid., Cont., and Dyn.*, Vol. 12, No. 1, 1989, pp. 71–81.

[3] Anthony, T. C., Wie, B., and Carroll, S., "Pulse-Modulated Control Synthesis for a Flexible Spacecraft," *J. of Guid., Cont., and Dyn.*, Vol. 13, No. 6, 1990, pp. 1014–1022.

[4] Hablani, H. B., "Self-Balanced Modal Control for Spacecraft Using Thrusters and Adaptive Bandpass Filters," *J. of Guid., Cont., and Dyn.*, Vol. 15, No. 3, 1992, pp. 587–596.

[5] Nakano, M. M., and Willms, R. L., "Space Shuttle On-Orbit Flight Control System," *Proc. of the AIAA Guid. and Cont. Conf.*, San Diego, CA, 1982, pp. 429–436.

[6] Vander Velde, W. E., and He, J., "Design of Space Structure Control Systems using On-Off Thrusters," *J. of Guid., Cont., and Dyn.*, Vol. 6, No. 1, 1983, pp. 53–60.

[7] Sackett, L. L., and Kirchwey, C. B., "Dynamic Interaction of the Shuttle On-Orbit Flight Control System with Deployed Flexible Payload," *Proc. of the AIAA Guid. and Cont. Conf.*, San Diego, CA, 1982, pp. 232–245.

[8] Penchuk, A. N., Hattis, P. D., and Kubiak, E. T., "A Frequency Domain Stability Analysis of a Phase Plane Control System," *J. of Guid., Cont., and Dyn.*, Vol. 8, No. 1, 1985, pp. 50–55.

[9] Kubiak, E. T., and Martin, M. W., "Minimum Impulse Limit Cycle Design to Compensate for Measurement Uncertainties," *J. of Guid., Cont., and Dyn.*, Vol. 6, No. 6, 1983, pp. 432–435.

[10] Martin, E., "Interaction of Payload and Attitude Controller in Space Robotic Systems," Master Thesis, Dept. of Mech. Eng., McGill University, Montreal, Canada, 1994.

[11] Chen, C. T., *Linear System Theory and Design*, Holt, Rinehart, and Winston, New York, 1984.

[12] Slotine, J.-J. E., and Li, W., *Applied Nonlinear Control*, Prentice Hall, Englewood Cliffs, N.J., 1991.

[13] Atherton, D. P., *Nonlinear Control Engineering*, Van Nostrand, New York, 1975.